OPTIMAL PROPERTIES OF SINGLE CONCAVE FRICTION PENDULUM BEARINGS FOR THE ISOLATION OF BRIDGES SUBJECTED TO FAR FIELD RECORDS

COMPDYN 2023
9th ECCOMAS Thematic Conference on
Computational Methods in Structural Dynamics and Earthquake Engineering
M. Papadrakakis, M. Fragiadakis (eds.)
Athens, Greece, 12-14 June 2023

OPTIMAL PROPERTIES OF SINGLE CONCAVE FRICTION PENDULUM BEARINGS FOR THE ISOLATION OF BRIDGES SUBJECTED TO FAR FIELD RECORDS

Elena Miceli[1], Diego Gino[1], Adolfo Ricioppo[1], Guglielmo Amendola[1], Luca Giordano[1] and Paolo Castaldo[1]

[1] Dipartimento di Ingegneria Strutturale, Edile e Geotecnica (DISEG), Politecnico di Torino, Corso Duca degli Abruzzi 24, Turin 10129, Italy
e-mail: {elena.miceli, diego.gino, adolfo.ricioppo, guglielmo.amendola, luca.giordano, paolo.castaldo}@polito.it

Abstract

The present study focuses on the analysis of the seismic performance of isolated bridges, equipped with single concave friction pendulum (FPS) bearings. The bridge is modelled through a six-degree-of-freedom system considering two FPS bearings placed on top of the rigid abutment and the elastic pier. The six equations of motion are analytically solved in order to obtain the response parameters normalized with respect to the peak ground acceleration-to-velocity ratio (PGA/PGV). In addition, a parametric analysis is conducted by varying some bridge properties. All these different bridges are then subjected to a set of 30 far field records having low and high PGA/PGV ratios to assess the seismic performance.

Keywords: Seismic isolation, bridges, FPS bearings, PGA/PGV.

1 INTRODUCTION

Nowadays, the safety of both structures and infrastructures is becoming an important issue. Regarding the context of seismic safety, both seismic isolation [1]-[3] and dissipation [4]-[7] are key strategies to reduce the seismic risk. Specifically, seismic isolation in case of infrastructures has the goal to decouple the inertia forces transmitted from the superstructures to the piers by increasing the period at the isolation level. The advantage of adopting the friction pendulum system (FPS) bearings are that the period of the isolation level becomes independent from the mass of the deck, the high restoring capacity and the low maintenance needs if compared to other isolators [8]-[9]. Many are the researches developed in the contest of seismically isolated bridges: for instance the development of numerical models to represent the behavior of the FPS isolators [10]-[14], the investigation of the effects of many geometrical and mechanical parameters within a parametric analysis on steel girder bridges isolated with FPS bearings [15], the identification of optimal properties of the isolators able at minimizing the substructure response [16]-[20]. However, in all these works the response in terms of optimal value for the friction coefficient is not independent from the seismic input characteristics.

The aim of the present study is to analyze the seismic performance of multi-span continuous deck isolated bridges, equipped with single concave friction pendulum system (FPS) bearings. A six-degree-of-freedom (dof) system is adopted to model the bridge, by considering 1 dof for the mass of the deck and 5 dofs corresponding to the lamped masses composing the pier. Two FPS isolators are placed on top of abutment, modeled as rigid and fixed, and of the elastic pier. The six equations of motion are analytically solved in order to obtain the response parameters normalized with respect to the peak ground acceleration-to-velocity ratio (*PGA/PGV*). In addition, a parametric analysis is conducted by varying some bridge properties. All these different bridges are then subjected to a set of 30 far field records having low and high *PGA/PGV* ratios.

2 NONDIMENSIONAL FORMULATION OF THE EQUATIONS OF MOTION

The multi-span continuous deck reinforced concrete (RC) isolated bridges are modeled through a six-degree-of-freedom (dof) system composed of 5 dofs associated to the lumped masses of the pier and 1 dof for the deck's mass, in line with [13],[19]-[20].

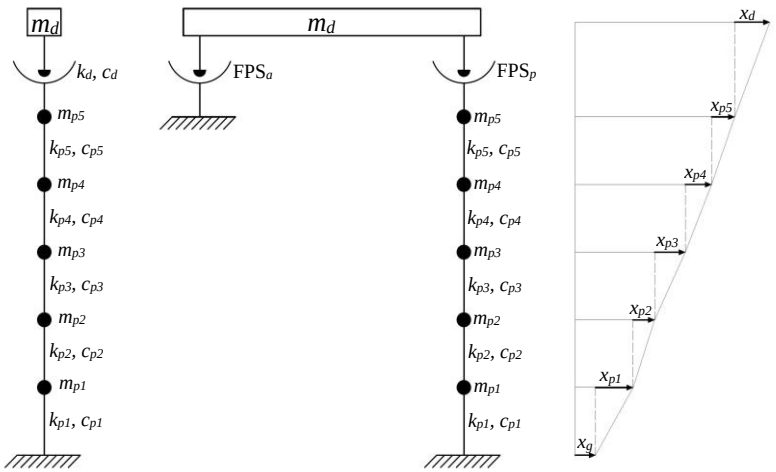

Figure 1 Scheme of the bridge model.

In detail, an FPS device is placed on top of the abutment and of the pier. The RC pier is modeled as flexible, while the RC abutment is considered rigid and fixed. The schematic representation of the bridge model together with the relative displacement of the dofs in longitudinal direction is shown in Figure 1. The equations of motion corresponding to the 6 dofs subjected to the horizontal component of the seismic input $\ddot{x}_g(t)$ are:

$$\begin{aligned}
&m_d\ddot{x}_d(t)+m_d\ddot{x}_{p5}(t)+m_d\ddot{x}_{p4}(t)+m_d\ddot{x}_{p3}(t)+m_d\ddot{x}_{p2}(t)+m_d\ddot{x}_{p1}(t)+c_d\dot{x}_d(t)+f_p(t)+f_a(t)=-m_d\ddot{x}_g(t)\\
&m_{p5}\ddot{x}_{p5}(t)+m_{p5}\ddot{x}_{p4}(t)+m_{p5}\ddot{x}_{p3}(t)+m_{p5}\ddot{x}_{p2}(t)+m_{p5}\ddot{x}_{p1}(t)-c_d\dot{x}_d(t)+c_{p5}\dot{x}_{p5}(t)+k_{p5}x_{p5}(t)-f_p(t)=-m_{p5}\ddot{x}_g(t)\\
&m_{p4}\ddot{x}_{p4}(t)+m_{p4}\ddot{x}_{p3}(t)+m_{p4}\ddot{x}_{p2}(t)+m_{p4}\ddot{u}_{p1}(t)-c_{p5}\dot{u}_{p5}(t)-k_{p5}u_{p5}(t)+c_{p4}\dot{x}_{p4}(t)+k_{p4}x_{p4}(t)=-m_{p4}\ddot{x}_g(t)\\
&m_{p3}\ddot{x}_{p3}(t)+m_{p3}\ddot{x}_{p2}(t)+m_{p3}\ddot{x}_{p1}(t)-c_{p4}\dot{u}_{p4}(t)-k_{p4}x_{p4}(t)+c_{p3}\dot{x}_{p3}(t)+k_{p3}x_{p3}(t)=-m_{p3}\ddot{x}_g(t)\\
&m_{p2}\ddot{x}_{p2}(t)+m_{p2}\ddot{x}_{p1}(t)-c_{p3}\dot{x}_{p3}(t)-k_{p3}x_{p3}(t)+c_{p2}\dot{x}_{p2}(t)+k_{p2}x_{p2}(t)=-m_{p2}\ddot{x}_g(t)\\
&m_{p1}\ddot{x}_{p1}(t)-c_{p2}\dot{x}_{p2}(t)-k_{p2}x_{p2}(t)+c_{p1}\dot{x}_{p1}(t)+k_{p1}x_{p1}(t)=-m_{p1}\ddot{x}_g(t)
\end{aligned} \tag{1}$$

where x_d stands for the deck displacement relative to the pier top, x_{pi} are the relative displacements of the ith lumped masses of the pier with respect to the lower one, m_d is the mass of the deck, m_{pi} is the mass of the ith lumped mass of the pier, while k_{pi} is the corresponding stiffness. The viscous damping coefficient for the bearing is c_d and c_{pi} is the viscous damping coefficient for the ith lamped masses of the pier; t is the time instant and the dots are used to indicate time derivative. All the lumped masses of the pier are assumed equal. The FPS isolators placed on top of the abutment and on the pier are subjected, respectively, to the restoring forces $f_a(t)$ and $f_p(t)$. These forces can be expressed as [8]:

$$\begin{aligned}
f_a(t)&=\frac{m_d g}{2}\left[\frac{1}{R_a}\left(x_d(t)+\sum_{i=1}^{5}x_{pi}\right)+\mu_a\left(\dot{x}_d+\sum_{i=1}^{5}\dot{x}_{pi}\right)\operatorname{sgn}\left(\dot{x}_d+\sum_{i=1}^{5}\dot{x}_{pi}\right)\right]\\
f_p(t)&=\frac{m_d g}{2}\left[\frac{1}{R_p}u_d(t)+\mu_p(\dot{x}_d)\operatorname{sgn}(\dot{x}_d)\right]
\end{aligned} \tag{2}$$

where the restoring forces of both devices derive from the sum of an elastic component and a viscous (i.e., dissipative) component. The only difference is that the force of the device on the abutment is function of the displacement and the corresponding velocity of the deck with respect to the ground, while for the isolator on the pier the restoring force depends on the displacement and the velocity of the deck with respect to the pier top. The elastic component derives from the pendular behavior of the devices. Furthermore, R_p and R_a are the radii of curvature of the isolators on top of, respectively, the pier and the abutment, g is the gravity constant, μ_a and μ_p are the sliding friction coefficient of the devices on top of the pier and the abutment, respectively. From equation (2) and assuming an equal radius of curvature for both devices (i.e., $R=R_a=R_p$), it can be derived the stiffness of the deck as $k_d = m_d g / R$. This also means that the fundamental period of the isolator does not depends on the mass of the deck but only on the geometrical characteristics of the isolator (i.e., $T_d = 2\pi\sqrt{R/\mathrm{g}}$). The sliding coefficients can be formulated as function of the sliding velocity as follows [8], [21]-[22]:

$$\mu(\dot{x}_d)=\mu_{\max}-(\mu_{\max}-\mu_{\min})\cdot\exp(-\alpha|\dot{x}_d|) \tag{3}$$

where μ_{min} and μ_{max} are the sliding friction coefficients at zero and large velocities, respectively, while α is a coefficient that governs the transition from low to large velocities. In this work the following is assumed: $\mu_{\min}=1/3\mu_{\max}$ and $\alpha=30$ according to [22].

3 PROBLEM'S PARAMETERS

In this work, many bridge properties vary in order to include different types of bridges. In particular it is assumed: 2 values of the mass ratio $\lambda = m_{pi}/m_d$ equal to 0.1 and 0.3; 2 values of the pier period T_p equal to 0.1 s and 0.2 s, 10 values of the ratio T_d/T_g from 0.5 to 8; 71 values of the normalized friction coefficient $\Pi_\mu^* = f_{\max} g/a_0$ from 0 to 0.8. In particular, a_0 is the seismic intensity measure that is assumed equal to the peak ground acceleration (i.e., $PGA=a_0$). In addition, it is assumed a fixed value for the viscous damping factors inherent to the pier and to the isolator, respectively, as follows: $\xi_{pi} = c_{pi}/2m_{pi}\,\omega_{pi} = 5\%$ and $\xi_d = c_d/2m_d\,\omega_d = 0\%$. In this way, combining all these parameters, a total of 2840 different bridge models are obtained.

Regarding the seismic input, two sets of non-frequent ground motions are considered: 15 FF records with high peak ground acceleration-to-velocity ratio (i.e., *PGA(g)/PGV>1.2g/m/s*) and reported in Table 1 and 15 FF records with low peak ground acceleration-to-velocity ratio (i.e., *PGA(g)/PGV<0.8g/m/s*) and reported in Table 2.

Earthquake	Date	Magnitudo	Distance (km)	Component	PGA(g)/PGV (g/m/s)
Parkfield California	June 27 1966	5.6	7	N65W	1.86
Parkfield California	June 27 1966	5.6	5	N85W	1.70
San Francisco California	Mar. 22 1957	5.25	11	S80E	2.28
San Francisco California	Mar. 22 1957	5.25	17	S09E	1.67
Helena Montana	Oct. 31 1935	6	8	N00E	2.03
Lytle Creek	Sep. 12 1970	5.4	15	S25W	2.06
Oroville California	Aug. 1 1975	5.7	13	N53W	1.91
San Fernando California	Feb. 9 1971	6.4	4	S74W	1.86
San Fernando California	Feb. 9 1971	6.4	26	S21W	1.72
NahanniN.W.T., Canada	Dec. 23 1985	6.9	7.5	LONG	2.38
Central Honshu Japan	Feb. 26 1971	5.5	27	TRANS	2.56
Near E. Coast of Honshu	May. 11 1972	5.8	33	N00E	2.43
Honshu Japan	Apr. 5 1966	5.4	4	N00E	2.43
Monte Negro Yugoslavia	Apr. 9 1979	5.4	12.5	N00E	2.63
Banja Luka Yugoslavia	Aug. 13 1981	6.1	8.5	N90W	2.31

Table 1 Set of 15 far field records with high *PGA(g)/PGV* ratios.

Earthquake	Date	Magnitudo	Distance (km)	Component	PGA(g)/PGV (g/m/s)
Long Beach California	Mar. 10 1933	6.3	59	N51W	0.41
Long Beach California	Mar. 10 1933	6.3	59	N39E	0.37
Lower Calif.	Dec. 30 1934	6.5	58	S00W	0.77
San Fernando California	Feb. 9 1971	6.4	40	N61W	0.52
San Fernando California	Feb. 9 1971	6.4	39	WEST	0.61
San Fernando California	Feb. 9 1971	6.4	41	S37W	0.69
San Fernando California	Feb. 9 1971	6.4	39	S90W	0.61
San Fernando California	Feb. 9 1971	6.4	38	N15E	0.54
San Fernando California	Feb. 9 1971	6.4	41	S38W	0.69
San Fernando California	Feb. 9 1971	6.4	32	S00W	0.62
Near E. Coast of Honshu	May 16 1968	7.9	290	N00E	0.68
Near E. Coast of Honshu	June 17 1973	7.4	112	N00E	0.75
Mexico Earthq.	Sep. 19 1985	8.1	135	S00E	0.65
Mexico Earthq.	Sep. 19 1985	8.1	333	N00E	0.70
Mexico Earthq.	Sep. 19 1985	8.1	379	N90W	0.36

Table 2 Set of 15 far field records with low *PGA(g)/PGV* ratios.

4 RESULTS AND DISCUSSION

To evaluate the performance of the different bridges, the equation of motions in (4) have been solved to assess the seismic performance. In particular, the response parameters are assumed to be the maximum normalized isolator response at the deck level (i.e., $\psi_{\mathrm{d,max}} = x_{\mathrm{d,max}}\omega_g^2/a_0$) and the maximum normalized pier response (i.e., $\psi_{\mathrm{p,max}} = x_{\mathrm{p,max}}\omega_g^2/a_0$), evaluated at the pier top, where $\omega_g = PGA/PGV$ represents the circular frequency of the ground motion.

Since each of the bridge model is subjected to a total of 30 FF natural ground motions, the responses are probabilistically treated. In particular, the responses are assumed to be lognormally distributed [23]-[32] and are assumed to have geometric mean (*GM*) and the dispersion (β) expressed as:

$$GM(D) = \sqrt[N]{d_1 \cdot \ldots \cdot d_N}$$
$$\beta(D) = \sigma_{\ln}(D) = \sqrt{\frac{\left(\ln d_1 - \ln(GM)\right)^2 + \ldots + \left(\ln d_N - \ln(GM)\right)^2}{N-1}} \tag{4}$$

where D is the response parameter, d_j is the j[th] realization of the response parameter and j=1,…,N with $N=30$ the total number of far field seismic records.

To evaluate the performance of the different bridges, the equation of motions in (4) have been solved in Matlab-Simulink [33].

The results of the *GM* of the peak normalized displacement of the pier top as function of the normalized friction coefficients are shown in Figure 2 and Figure 3 for FF field records with, respectively, high and low *PGA/PGV* ratios.

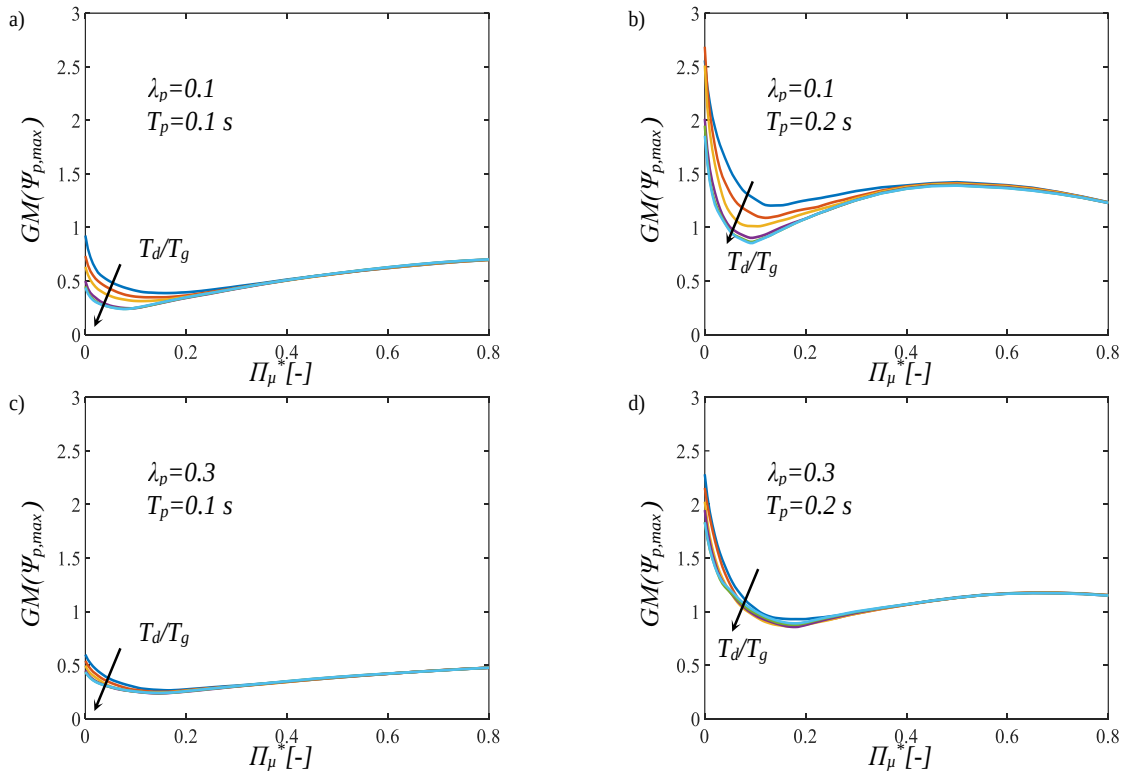

Figure 2 Geometric mean of the peak response of the pier top with respect to Π_μ^* for FF records with high *PGA/PGV* ratios.

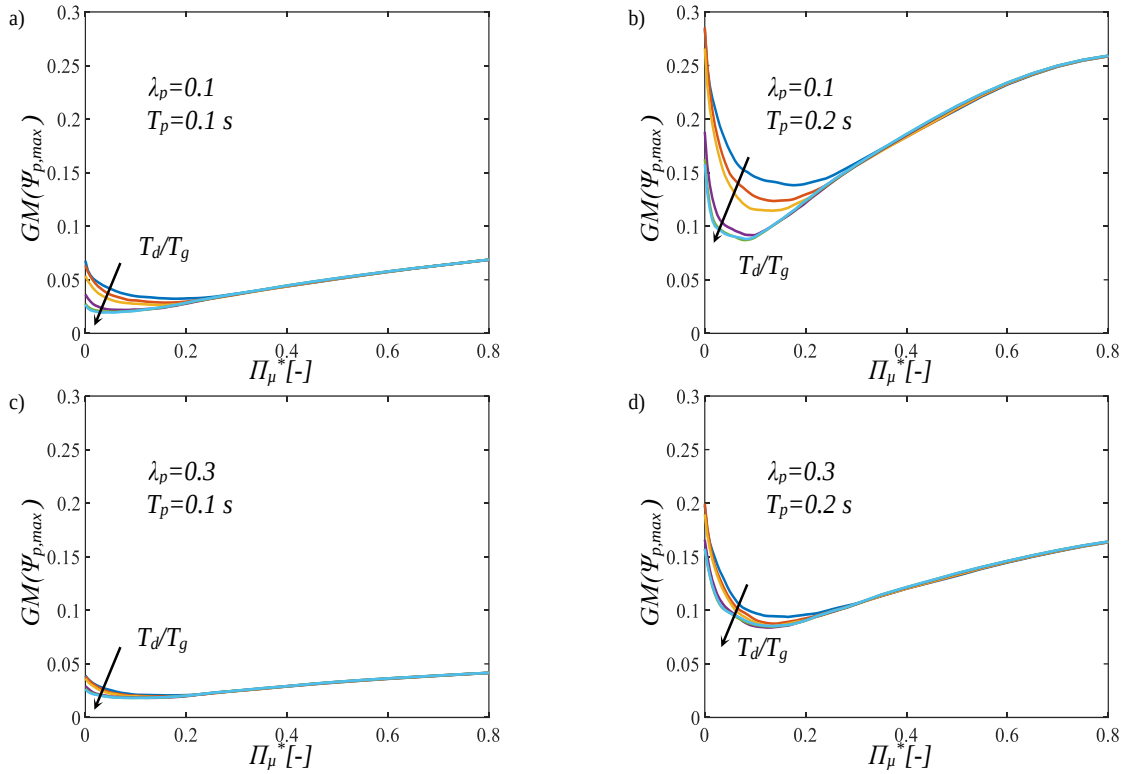

Figure 3 Geometric mean of the peak response of the pier top with respect to Π_μ^* for FF records with low *PGA/PGV* ratios.

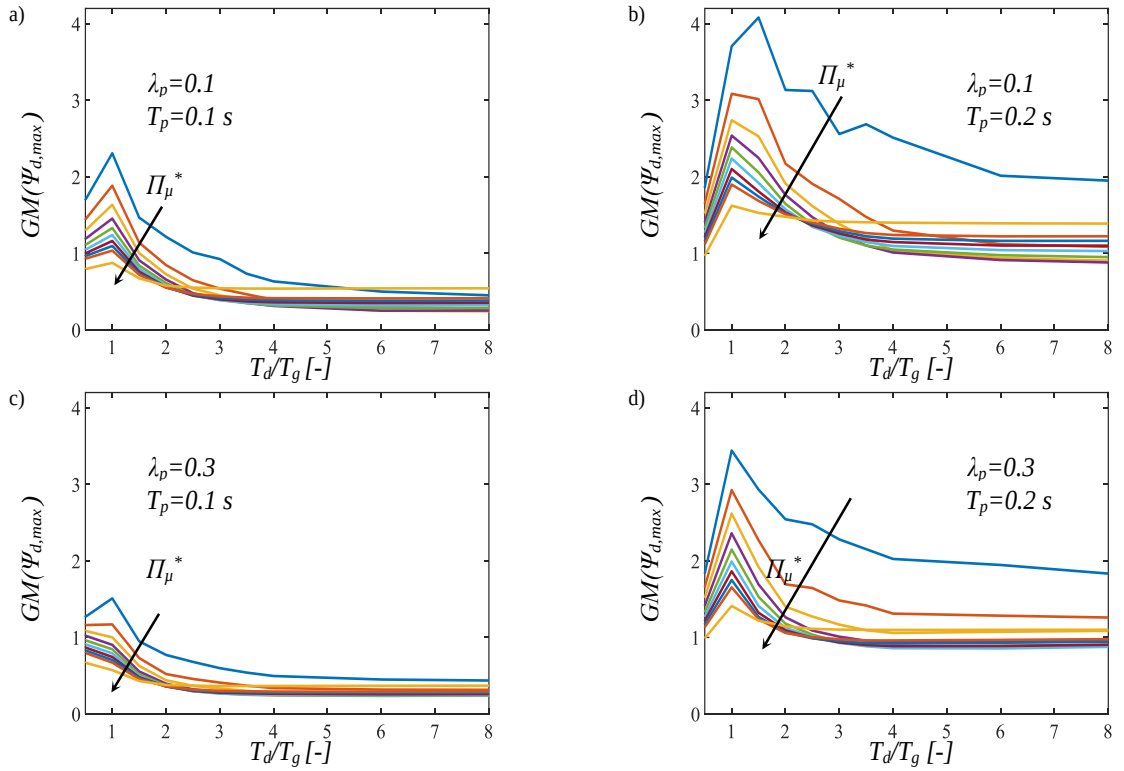

Figure 4 Geometric mean of the peak response of the deck with respect to T_d/T_g for FF records with high *PGA/PGV* ratios.

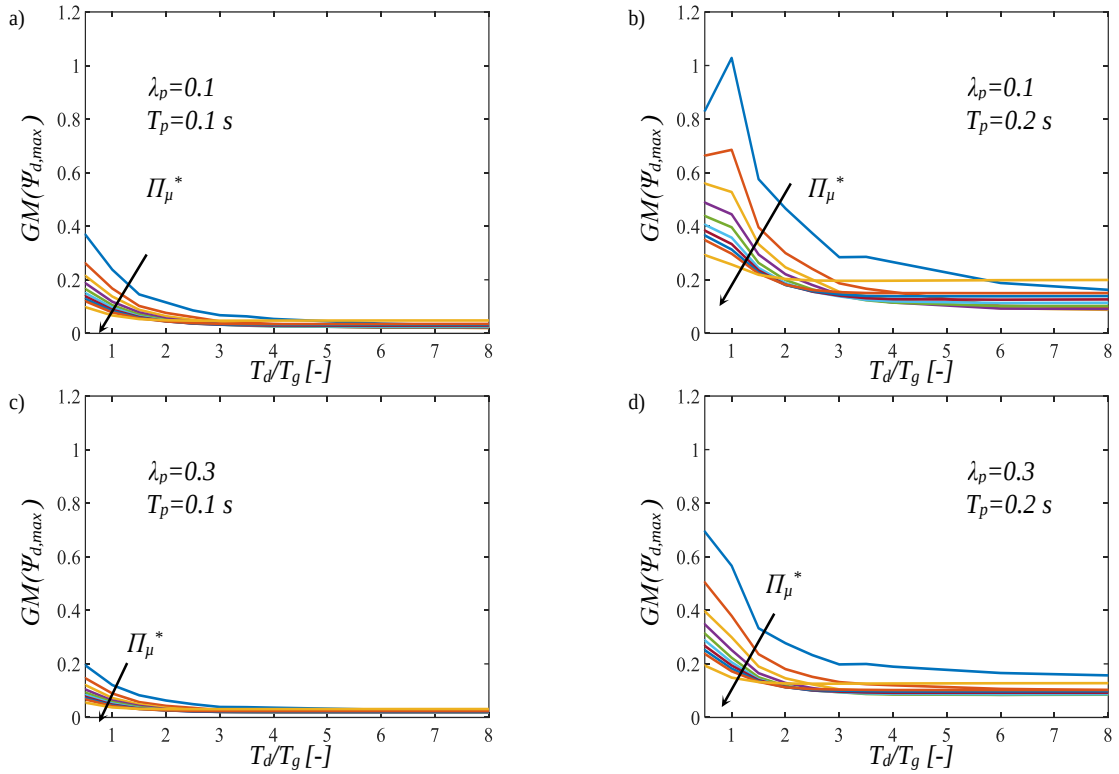

Figure 5 Geometric mean of the peak response of the deck with respect to T_d/T_g for FF records with low *PGA/PGV* ratios.

The response is shown for fixed values of the other parameters (i.e., T_d/T_g, T_p and λ_p). In general, the geometric mean of the substructure response increases for lower T_d/T_g values, increases for larger T_p values and increases for lower values of λ_p, since this reduction causes an increase in the forces transmitted from the superstructure to the pier. In addition, larger *PGA/PGV* ratios are more demanding. The interesting aspect is that the response of $\psi_{p,max}$ tends first to decrease and then to increase for larger normalized friction coefficient Π_μ^* and this trend is maintained independently from the values assumed by the other parameters. This result derives from two counteracting effects: on the one hand the increase of the friction reduces the inertia forces transmitted from the deck to the substructure and, on the other hand, if the friction increases higher modes participates to the response increasing its value. This suggests the possibility to identify optimal values of the friction coefficient able at minimizing the substructure response. These minimum values are also obtained in similar ranges if the other structural parameters change but also by varying the record selection. In addition, it is suggested to perform further analyses in order to find numerical expressions for the optimal friction coefficient.

In Figure 4 and Figure 5, it is shown the peak normalized response of the deck as function of the ratio T_d/T_g for FF field records with, respectively, high and low *PGA/PGV* ratios. The response is shown for fixed values of the other parameters (i.e., Π_μ^*, T_p and λ_p). It is possible to observe that there is an increase of the deck response with T_d/T_g, followed by a decrease, especially, for low Π_μ^*. This response is similar to the displacement response spectrum of an

isolated mass. In addition, $GM(\psi_{d,\max})$ is mainly influenced by the normalized friction coefficient Π_{μ}^{*} since its growth reduces the deck response since larger energy dissipation is obtained. Regarding the other parameters, the deck response is not particularly influenced by the other two structural parameters. Furthermore, larger *PGA/PGV* ratios result to be more demanding also for the isolation response.

5 CONCLUSIONS

The present investigation aims at evaluating the seismic response of multi-span continuous deck bridges equipped with single concave FPS devices. A parametric analysis is elaborated by varying many parameters (i.e., pier period, isolated period, mass of the pier with respect to the mass of the deck, friction coefficient), in order to obtain different bridge models. The equations of motion have been analytically treated in order to obtain a non dimensional response. In particular, the response of the substructure (i.e., the pier) and of the isolation system have been normalized with respect to the ground motion characteristics through the acceleration-to-velocity (*PGA/PGV*) ratio. The set of records have been selected in order to include 30 far field non-frequent natural ground motions with high and low acceleration-to-velocity (*PGA/PGV*) ratio. Results have shown the existence of an optimal value of the normalized friction coefficient able to minimize the peak normalized substructure displacement.

ACKNOWLEDGEMENTS

This work is also part of the collaborative activity developed by the authors within the framework of the "PNRR": VS3 "Earthquakes and Volcanos" - WP3.6 and SPOKE 7 "CCAM, Connected Networks and Smart Infrastructure" - WP4.

REFERENCES

[1] A. Ghobarah, H.M. Ali, Seismic performance of highway bridges. *Engineering Structures*, **10**(3), 157-166, 1988.

[2] P. Tsopelas, M.C. Constantinou, S. Okamoto, S. Fujii, D. Ozaki, Experimental study of bridge seismic sliding isolation systems. *Engineering Structures*, **18**(4), 301-310, 1996.

[3] R.S. Jangid, Seismic Response of Isolated Bridges. *Journal of Bridge Engineering*, **9**(2), 156-166, 2004.

[4] P. Colajanni, L. La Mendola, A. Monaco, S. Pagnotta, Seismic performance of earthquake-resilient RC frames made with HSTC beams and friction damper devices. *Journal of Earthquake Engineering*, **26**(15), 7787-7813, 2022.

[5] Tsiavos, A., Amrein, P., Bender, N. et al. Compliance-based estimation of seismic collapse risk of an existing reinforced concrete frame building. *Bull Earthquake Eng*, **19**, 6027–6048, 2021.

[6] Tsiavos, A., Kolyfetis, D., Panzarasa, G. et al. Shaking table investigation of a low-cost and sustainable timber-based energy dissipation system with recentering ability. *Bull Earthquake Eng*, 2022, https://doi.org/10.1007/s10518-022-01464-2.

[7] P. Colajanni, L. La Mendola, A. Monaco, S. Pagnotta, Design of RC joints equipped with hybrid trussed beams and friction dampers. *Engineering Structures*, **227**, 111442, 2021.

[8] V. Zayas, S. Low, S. Mahin, A simple pendulum technique for achieving seismic isolation. *Earthquake Spectra*, **6(2)**, 317-333, 1990.

[9] L. Su, G. Ahmadi, I. Tadjbakhsh, Comparative Study of Base Isolation Systems. *Journal of Engineering Mechanics*, **115**(9), 1976-1992 (1989).

[10] JL. Almazàn, J.C. De la Llera, Physical model for dynamic analysis of structures with FPS isolators. *Earthquake Engineering and Structural Dynamics*, **32**(8):1157–1184, 2003.

[11] G. Mosqueda, A.S. Whittaker, G.L. Fenves, Characterization and modeling of Friction Pendulum bearings subjected to multiple components of excitation. *Journal of Structural Engineering*, **130**(3), 433-442, 2004.

[12] R. S. Jangid, Computational numerical models for seismic response of structures isolated by sliding systems. *Structural Control and Health Monitoring*, **12**, 117–137, 2005.

[13] R.S. Jangid, Stochastic response of bridges seismically isolated by friction pendulum system. *Journal of Bridge Engineering*, **13**(4), 319, 2008.

[14] L. Landi, G. Grazi, P. Diotallevi, Comparison of different models for friction pendulum isolators in structures subjected to horizontal and vertical ground motions. *Soil Dynamics and Earthquake Engineering*, **81**, 75-83, 2016.

[15] M. Eröz, R. DesRoches, The influence of design parameters on the response of bridges seismically isolated with the friction pendulum system (FPS). *Engineering structures*, **56**, 585-599, 2013.

[16] R.S. Jangid, Optimum frictional elements in sliding isolation systems. *Computers and Structures*, **76**(5),651–661, 2000.

[17] R.S. Jangid, Optimum friction pendulum system for near-fault motions. *Engineering Structures*, **27**(3), 349–359, 2005.

[18] P. Castaldo, M. Ripani, R. Lo Piore, Influence of soil conditions on the optimal sliding friction coefficient for isolated bridges. *Soil Dynamics and Earthquake Engineering*, **111**, 131–148, 2018.

[19] P. Castaldo, G. Amendola, Optimal Sliding Friction Coefficients for Isolated Viaducts and Bridges: A Comparison Study. *Structural Control and Health Monitoring*, **28**(12), 2838, 2021, doi:10.1002/stc.2838.

[20] P. Castaldo, G. Amendola, Optimal DCFP bearing properties and seismic performance assessment in nondimensional form for isolated bridges. *Earthquake Engineering and Structural Dynamics*, **50**(9), 2442-2461, 2021, doi: 10.1002/eqe.3454.

[21] A. Mokha, M.C. Constantinou, A.M. Reinhorn, Teflon Bearings in Base Isolation. I: Testing. *Journal of Structural Engineering*, **116**(2), 438-454, 1990.

[22] M.C. Constantinou, A.S. Whittaker, Y. Kalpakidis, D.M. Fenz, G.P. Warn, Performance of Seismic Isolation Hardware Under Service and Seismic Loading. *Technical Report MCEER-07-0012*, 2007.

[23] P. Castaldo, E. Tubaldi, Influence of Ground Motion Characteristics on the Optimal Single Concave Sliding Bearing Properties for Base-isolated Structures. *Soil Dynamics and Earthquake Engineering*, **104**, 346-64, 2018.

[24] R. Troisi, G. Alfano, Proximity and inter-firm corruption: A transaction cost approach. *Small Business Economics*, **60**, 1105–1120, 2022.

[25] R. Troisi, P. Di Nauta, P. Piciocchi, Private corruption: An integrated organizational model. *European Management Review*, **19**(3), 476-486, 2022.

[26] R. Troisi, Illegal land use by Italian firms: An empirical analysis through the lens of isomorphism. *Land Use Policy*, **121**, 106321, 2022.

[27] R. Troisi, G. Alfano, Is regional emergency management key to containing COVID-19? A comparison between the regional Italian models of Emilia-Romagna and Veneto. *International Journal of Public Sector Management*, **35**(2), 195-210, 2022.

[28] R. Troisi, G. Alfano, Firms' crimes and land use in Italy. An exploratory data analysis *New Metropolitan Perspectives: Knowledge Dynamics and Innovation-driven Policies Towards Urban and Regional Transition*, Reggio Calabria, Italy, May 25-27, 2021.

[29] R. Troisi, G. Alfano, The re-election of corrupt mayors: context, relational leadership and level of corruption. *Local Government Studies*, **49**(1), 204-225, 2022.

[30] R. Troisi, S. De Simone, M. Vargas, M. Franco, The other side of the crisis: organizational flexibility in balancing Covid-19 and non-Covid-19 health-care services. *BMC Health Services Research*, **22**(1), 1096, 2022.

[31] R. Troisi, G. Alfano, Is "justice hurried actually justice buried"? An organisational perspective of the Italian criminal justice. *International Journal of Public Sector Management*, **36**(1), 94–109, 2023.

[32] A. Nese, R. Troisi, Individual preferences and job characteristics: an analysis of cooperative credit banks. *Labour*, **28**(2), 233-249, 2014.

[33] Math Works Inc., *MATLAB-High Performance Numeric Computation and Visualization Software. User's Guide*, Natick (MA), USA, 1997.